Quantitative assessment of the structure of Ge 20 Te 73 I 7 chalcohalide glass by first-principles molecular dynamics

Assil Bouzid, Tan-Lien Pham, Ziyad Chaker, Mauro Boero, Carlo Massobrio, Young-Han Shin, Guido Ori

PHYSICAL REVIEW B **00**, 004200 (2021)

Quantitative assessment of the structure of $Ge_{20}Te_{73}I_7$ chalcohalide glass by first-principles molecular dynamics

Assil Bouzid,[1,*] Tan-Lien Pham,[2] Ziyad Chaker,[3] Mauro Boero,[4] Carlo Massobrio,[4] Young-Han Shin,[2] and Guido Ori[4,†]

[1]*Institut de Recherche sur les Céramiques, UMR 7315 CNRS-Univesité de Limoges, Centre Européen de la Céramique, 12 rue Atlantis 87068 Limoges Cedex, France*

[2]*Multiscale Materials Modeling Laboratory, Department of Physics, University of Ulsan, Ulsan 44610, Republic of Korea*

[3]*International Center for Materials Nanoarchitectonics (WPI-MANA), National Institute for Materials Science (NIMS), 3-13 Sakura, Tsukuba, Ibaraki 305-0003, Japan*

[4]*Université de Strasbourg, CNRS, Institut de Physique et Chimie des Matériaux de Strasbourg, UMR 7504, F-67034 Strasbourg, France*

(Received 16 December 2020; revised 2 March 2021; accepted 4 March 2021; published xxxxxxxxxx)

First-principles molecular dynamics, within the density functional theory framework, is employed to assess the structural properties of the chalcohalide glass $Ge_{20}Te_{73}I_7$ (gGTI). The calculated total x-ray and neutron structure factors are in quantitative agreement with the experimental counterparts. Glassy gGTI features a predominantly Ge-centered tetrahedral network moderately altered by iodine atoms. Compared to glassy $Ge_{20}Te_{80}$, gGTI shows a substantial decrease in the number of Ge-Te bonds as the presence of I leads to a breaking of the Ge-Te connections and favors the formation of Ge-I terminations where iodine atoms are onefold. Furthermore, we remark on a concomitant increase of mixed $GeTe_{4-x}I_x$ tetrahedra and $GeTe_{3-x}I_x$ trigonal pyramidal units. A minor yet not-negligible fraction of iodine atoms forms Te-I bonds. Breaking of Ge-Te connections and formation of terminal Ge(Te)-I bonds results in a reduced average coordination number associated with an increase of undercoordinated Ge at the expense of fourfold coordinated Ge atoms. The analysis of chains and rings statistics reveals the presence of both linear and cross-linked chains made of Te and five-members rings containing at least one Te-Te or one Ge-Ge homopolar bond.

DOI: 10.1103/PhysRevB.00.004200

I. INTRODUCTION

Chalcogenide glasses have a wealth of applications in far-infrared optics, optoelectronic devices, and photonics because of their broad transmission window (from the visible-near IR range to the mid-IR), low-phonon energy, and high chemical durability [1–4]. In particular, telluride-based glasses have a wide transparency window in the whole infrared range up to 28 μm, crucial for applications in space optics, biochemistry, and gas sensing [5,6]. To reduce their intrinsic strong tendency to crystallize, telluride-based glasses are usually combined with suitable chemical elements [7]. In this respect, to prevent crystallization (i.e., devitrification) $Ge_{20}Te_{80}$ (commonly identified with its reduced glass composition formula $GeTe_4$, gGT4 in what follows) can be modified with the addition of elements enhancing the temperature separation ΔT between the glass transition T_g and the crystallization temperature T_x [8]. Danto *et al.* observed that the addition of Ga in glassy $Ga_{10}Ge_{15}Te_{75}$ improved the glass stability by an increase of ΔT up to 113 K with respect to 77 K in gGT4 [9]. Yet such an increase of ΔT is still insufficient to prevent parasitic nucleation processes of Te, thus undermining potential applications in optical fibers. Wilhelm *et al.* has shown that glassy $Ge_{20}Te_{73}I_7$ (gGTI hereafter) is stable with an improved far-infrared-transmitting performance in the 2–22 μm range increasing ΔT to 124 K (T_g: 413 K and 423 K; T_x: 490 K and 547 K for gGT4 and gGTI) [6,10]. Within the family of chalcohalide glasses, other compounds such as Ga-Ge-Te-I and Ge-Te-Ag-I received special attention, but they did not perform better than gGTI in terms of glass stability [11–13].

In view of the above findings, it appears that one needs to better understand the interplay between the role of iodine, glass structure, and the glass-forming ability in these systems, with special emphasis on the strong tendency to crystallization driven by Te. In this respect, the structural mechanism of halogens incorporation into the chalcogenide glass network and its interaction with the other components is still elusive, receiving renewed attention for both gGTI and other chalcohalide glasses such as As-Se-I [14,15].

Former atomic-scale modeling simulations of gGTI and other Te-rich Te-Ge-X (X = I, Se, Ga) glasses were performed by Jóvári *et al.* [7] using constrained reverse Monte Carlo (cRMC) simulations, combining experimental x-ray and neutron diffraction and extended x-ray absorption fine structure datasets. The produced gGTI glass model was described as made of $GeTe_4$ and $GeTe_3I$ tetrahedral connected by Te-Te bonds. To obtain this picture, Ge and I atoms were constrained to have four and one neighbors, respectively. This assumption was driven by the consideration that both Ge and I did not show any coordination defect in gGTI [7]. More

*assil.bouzid@unilim.fr
†guido.ori@ipcms.unistra.fr

recent results by the same group using unconstrained RMC (uRMC) simulations showed a better agreement with the experimental data in terms of bond lengths and coordination for both Ge-Te and Ga-Ge-Te based glasses [16,17]. By resorting to first-principles molecular dynamics (FPMD) simulations, within the density functional theory (DFT) framework, we were able to accurately model binary and ternary chalcogenide glasses, namely sulfides [18,19], selenides [20], and tellurides [21–23]. A systematic assessment of the impact of both the van der Waals (vdW) interactions and the exchange-correlation (XC) functional allowed us to achieve a quantitative description for the structure of gGT4 [24] and $Ga_{10}Ge_{15}Te_{75}$ [25] glasses, substantiated by an unprecedented agreement with x-ray and neutron scattering experiments. Our methodology is further legitimated by a direct comparison with the more recent results by Jóvári *et al.* [16,17], which are in better agreement with our FPMD data than their former results.

For these reasons, we are convinced we can safely apply the same FPMD method to chalcohalide systems, since no models of this kind have ever been proposed for this family of systems. To fill this gap, we report in this paper the results of a thorough FPMD study devoted to the structure of gGTI. Structural properties are analyzed in detail and compared with available experimental data [7] as well as with our former results on gGT4 [24]. For sake of completeness, we also compare our FPMD results on gGT4 [24] with the new set of experimental data by the team of Jóvári [16,17] on $Ge_{18.7}Te_{81.3}$ and $Ge_{23.6}Te_{76.4}$ glasses.

Our paper is organized as follows. Section II reports on the methodology and the model systems employed. Section III is organized in five subsections, and it is devoted to a critical analysis and discussion of our FPMD results. The first two feature the comparison between theory and experiments for the total structure factor $S(k)$ and the pair correlation functions $g(r)$. Then, we analyze the coordination numbers for each chemical species composing the system, along with bond angles distributions and bond order parameters. The analysis of rings and chains statistics can be found in a final subsection. Concluding remarks are collected in Sec. IV.

II. COMPUTATIONAL METHODS AND MODEL CONSTRUCTION

We make use of FPMD in the Car-Parrinello [26] version (CPMD) [27]. The XC exchange-correlation functional adopted is composed by the Becke [28] and the Lee-Yang-Parr [29] (BLYP) functionals for exchange and correlation, respectively. The valence-core interaction is described by norm-conserving Troullier-Martins (TM) pseudopotentials (PPs) [30]. Valence electrons are accounted for in terms of a plane-wave basis set with an energy cutoff of 40 Ry. The Brillouin zone sampling is limited to the 1` point as it is customary for disordered systems. A fictitious electron mass of 850 a.u. and a time step $\Delta t = 0.12$ fs ensured a good numerical control of the constant of motion. The ionic temperature was controlled with a Nosé-Hoover [31–33] thermostat chain [34], whereas for the fictitious electronic kinetic energy we used a Blöchl-Parrinello thermostat [35] with a target kinetic energy of 0.08 a.u. Van der Waals long-range dispersion forces were included via the DFT-D2 formula of Grimme [36].

Two $Ge_{20}Te_{73}I_7$ glass models (hereafter termed as $gGTI_1$ and $gGTI_2$) were generated by quenching from the melt. The two initial configurations consisted of disordered systems made of 480 atoms (96 Ge, 350 Te, and 34 I) in a cubic simulation cell of side 25.5045 Å, corresponding to an atomic number density of 0.02893 $Å^{-3}$. Given this value, the two final glass systems at the end of the thermal cycle ($T = 300$ K) had a negligible residual pressure (<0.8 GPa). Our selected density is 4.5% higher than the experimental density (5.36 g cm^{-3}, see Ref. [37]). Overall, the choice of working at negligible pressure instead of imposing the experimental density is more rewarding in terms of comparison with experimental structural data. Periodic boundary conditions were applied throughout the FPMD simulations. Both models underwent a thermal cycle via canonical NVT simulations, according to the following protocol. For $gGTI_1$ the simulations lasted 5 ps at $T = 300$ K, 5 ps at $T = 600$ K, 16 ps at $T = 900$ K, 10 ps at $T = 600$ K, and 34 ps at $T = 300$ K. For $gGTI_2$, the corresponding quantities were 2.5 ps at $T = 300$ K, 2.5 ps at $T = 600$ K, 10 ps at $T = 900$ K, 8 ps at $T = 600$ K, and 12 ps at $T = 300$ K. We remark that at 900 K both systems are characterized by pair correlation functions reminiscent of the liquid state, ensuring an effective loss of memory of the initial configurations. In what follows, the results are presented as time-average values on each distinct set of coordinates on the last part (10 ps) of the thermal cycles at $T = 300$ K. Representative configurations of gGTI models and raw trajectory data are available at the European Center of Excellence Novel Materials Discovery (CoE-NOMAD) repository (see Ref. [38]).

III. RESULTS AND DISCUSSION

A. Total structure factors

The total neutron structure factor $S_T^n(k)$ is defined by

$$S_T^n(k) - 1 \equiv \sum_{\alpha=1}^{n}\sum_{\beta=1}^{n} \frac{c_\alpha c_\beta b_\alpha b_\beta}{\langle b\rangle^2}\left[S_{\alpha\beta}^{\mathrm{FZ}}(k) - 1\right], \qquad (1)$$

where α and β denote the chemical species, n is the number of the different chemical species, c_α and b_α are the atomic fraction and coherent neutron scattering length of the chemical specie α, $\langle b\rangle = c_\alpha b_\alpha + c_\beta b_\beta$ is the mean coherent neutron scattering length, and $S_{\alpha\beta}^{\mathrm{FZ}}(k)$ is a Faber-Ziman (FZ) partial structure factor.

$$S_{\alpha\beta}^{\mathrm{FZ}}(k) - 1 \equiv \frac{4\pi n_0}{k}\int_0^\infty r\,[g_\alpha b_\beta(r) - 1]\sin(kr)\,dr \qquad (2)$$

In the real space, the corresponding quantity is the total pair distribution function:

$$g_T(r) - 1 = \frac{1}{2\pi^2 n_0 r}\int_0^\infty k\,[S_T(k) - 1]\sin(kr)\,dk$$
$$= \sum_{\alpha=1}^{n}\sum_{\beta=1}^{n} \frac{c_\alpha c_\beta b_\alpha b_\beta}{\langle b\rangle^2}[g_{\alpha\beta}(r) - 1], \qquad (3)$$

where n_0 is the atomic number density and $g_{\alpha\beta}(r)$ is a partial pair distribution function.

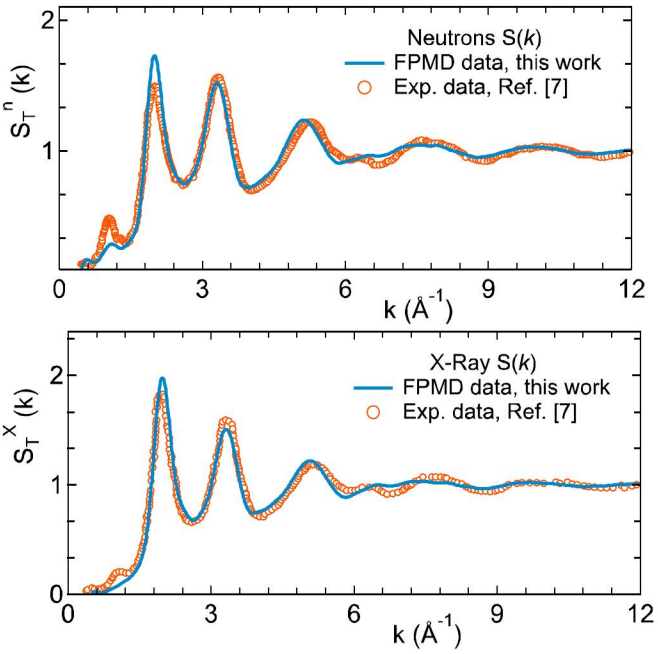

FIG. 1. Calculated total neutron and x-ray structure factors S(k) of glassy gGTI at 300 K (blue solid line). The experimental data (orange open circles) are taken from the work of Jóvári *et al.* [7].

Analogously, the total x-ray structure factor $S_T^X(k)$ is defined by:

$$S_T^X(k) - 1 = \sum_{\alpha=1}^{n}\sum_{\beta=1}^{n} \frac{c_\alpha c_\beta f_\alpha f_\beta}{|\langle f\rangle^2|}\left[S_{\alpha\beta}^{FZ}(k) - 1\right], \qquad (4)$$

where f_α and f_β are the corresponding scattering factors.

The calculated total neutron and x-ray structure factors $S_T^n(k)$ and $S_T^X(k)$ of gGTI simulated at 300 K are shown in Fig. 1 and compared with their experimental counterparts for an identical composition [7]. Additional information is available in Fig. S1 of the Supplemental Material (SM) for $S_T^n(k)$ and $S_T^X(k)$ [39]. We remark the excellent agreement for the shapes of $S_T^n(k)$ and $S_T^X(k)$ over the entire k range. The only discrepancies are related to a less pronounced first sharp diffraction peak (FSDP) at ∼1 Å^{-1} and a slight overestimate of the intensity of the second peak at ∼2.1 Å^{-1}. The presence of a feature at the FSDP location is indicative of a limited degree of intermediate range order for the gGTI system, in a way analogous to what found in the $Ga_{10}Ge_{15}Te_{75}$ [25] glass.

The quantitative agreement with the experimental data [7] is confirmed by a remarkable goodness-of-fit R_x parameter [40], defined as:

$$R_\chi = \left\{\frac{\sum_i [T_{exp}(r_i) - T_{FPMD}(r_i)]^2}{\sum_i T_{exp}^2(r_i)}\right\}^{1/2}, \qquad (5)$$

where $T(r_i)$ denotes a real space correlation function. For gGTI, we obtained $R_x = 5.91\%$ and 5.53% for neutron and x-ray structure factors, respectively. These R_x values are in line with the degree of quantitative agreement found with former results on gGT4, $R_x = 8.9\%$ [7]. In the SM section we have added a comparison of the average total neutron structure factor $S_T^n(k)$ of gGT4 with the original and new set of experimental data of Jóvári *et al.* [7,16,41] for $Ge_{18.7}Te_{81.3}$ and $Ge_{23.6}Te_{76.4}$ glasses (Fig. S2: $R_x = 7.07\%$ and 6.55%, respectively). The agreement found is worth pointing out.

TABLE I. Bond lengths r_{ij} (in Å) in terms of position of the first maximum of the pair correlation functions $g_{ij}(r)$, partial coordination numbers n_{ij} obtained by integration of g_{ij} up to the first minimum, coordination numbers n_i, and average coordination number $\bar{n}$. We include the percentage of Ge and Te atoms involved in homopolar bonds N_{GeGe} and N_{TeTe}, and the percentages of Ge atoms making edge-sharing (ES) or corner-sharing (CS) connections. The statistical uncertainties on the reported values are ±0.03 Å and ±0.05 for distances and coordinations, respectively.

	$Ge_{18.7}Te_{81.3}$[a] Expt.	$Ge_{23.6}Te_{76.4}$[a] Expt.	GT4[b] FPMD	GTI[c] Expt.	GTI[d] FPMD
r_{GeGe}		2.45	2.43		2.43
r_{GeTe}	2.61	2.61	2.59	2.60	2.61
r_{TeTe}	2.76	2.75	2.84	2.70	2.83
r_{GeI}				2.58	2.54
r_{TeI}					2.86
n_{GeGe}		0.44	0.37		0.33
n_{GeTe}	4.10	3.66	3.64	3.73	3.21
n_{TeTe}	0.94	0.93	1.40	1.00	1.39
n_{GeI}				0.29	0.28
n_{TeI}				0.03	0.04
n_{Ge}	4.10	4.00	3.97	3.97	3.81
n_{Te}	2.00	2.06	2.31	2.04	2.32
n_I				0.63	1.24
$\bar{n}$	2.39	2.53	2.65	2.32	2.54
N_{GeGe}			30.30		25.32
N_{TeTe}			80.26		81.06
N_{Ge}^{CS}			53.07		61.16
N_{Ge}^{ES}			16.60		13.52

[a]Combining experiments and uRMC calculations, from Ref. [16].
[b]From Ref. [24], FPMD simulations.
[c]Combining experiments and cRMC calculations, from Ref. [7].
[d]This work, FPMD simulations.

B. Total and partial pair correlation functions

The calculated total and partial pair correlation functions (PCFs) $g_{\alpha\beta}(r)$ for gGTI are shown in Fig. 2. A comparison is provided with gGT4 obtained by our team with the same computational approach [24]. In Fig. S3 of the SM we also provide the total and partial PCFs for the two distinct trajectories of gGTI. The trends exhibited by $g_{\alpha\beta}(r)$ for the two models are rather similar over the whole range of distances. The picture emerging from the PCFs is quantitatively complemented by the nearest-neighbor distances given in Table I, intended as the first peak position averaged over the two available trajectories.

In what follows, we first consider the FPMD results for gGT4 by taking advantage of the recent work by Jóvári *et al.* for $Ge_{18.7}Te_{81.3}$ and $Ge_{23.6}Te_{76.4}$ glasses [16]. Nearest-neighbor distances of Ge-Te and Ge-Ge (2.59 Å and 2.43 Å) are reproducing within the statistical uncertainty the values of 2.61 Å and 2.45 Å reported in Ref. [16]). The only noticeable difference is found in the Te-Te distances (2.84 vs 2.75–2.76 Å). However, this is compatible with the broad distribution

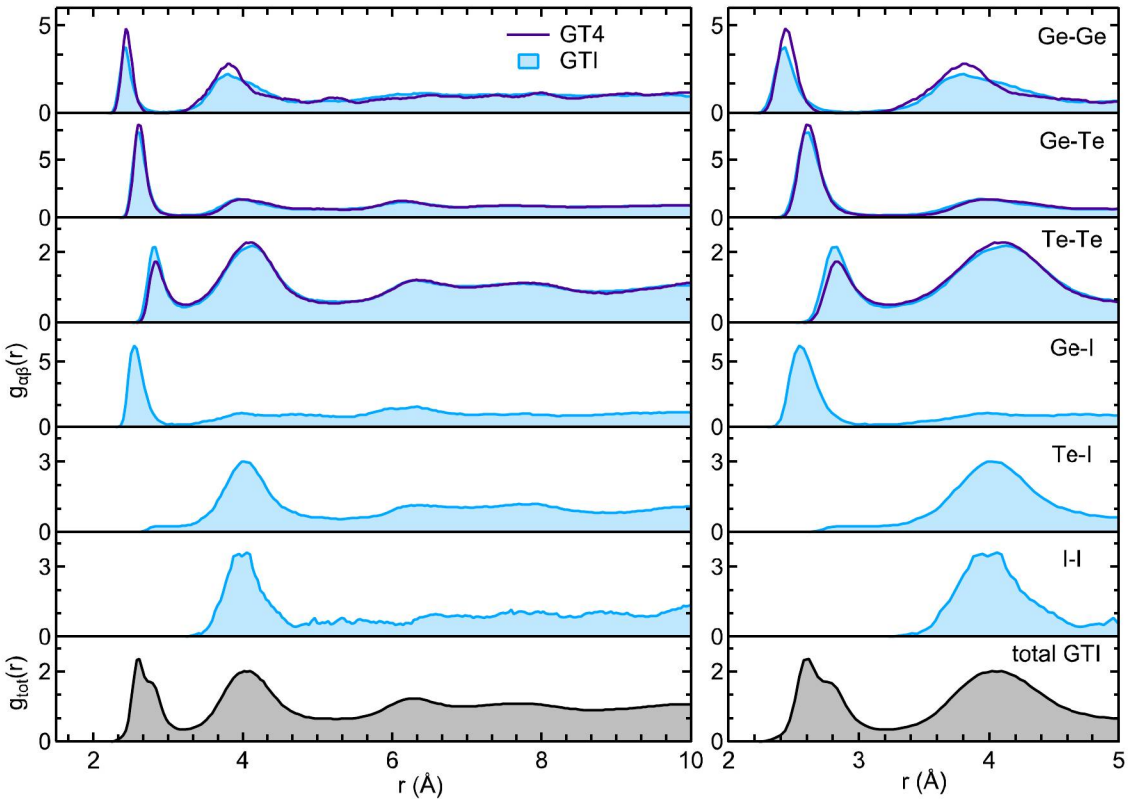

FIG. 2. Left: Calculated total and pair correlation functions $g_{\alpha\beta}(r)$ (α, β = Ge, Te, I) for gGTI system (blue and black solid lines). The $g_{\alpha\beta}(r)$ data of gGT4 is also shown (purple solid line) [24]. Right: Zoom-in within the 2–5 Å range.

of Te-Te distances reported in the literature for telluride glasses. Namely, values found are in the range 2.77–2.82 Å in glassy Ge_x-Te_{100-x} by EXAFS [42,43] and 2.70–2.79 Å by a combination of x-ray diffraction, EXAFS, and RMC [44,45]. Also, 2.79–2.80 Å values were reported for Ge-Ga-Te [46] and 2.77–2.79 Å for Ge-Te-Ag-I glasses by the same combination of measurements [47]. By focusing on the atomic structure, we first observe that the pair correlation functions PCFs of gGTI look to a very good extent similar to those of gGT4. However, for gGTI, a decrease of the intensity appears in the first main peaks of both Ge-Te and Ge-Ge PCFs, while there is an increase in the Te-Te PCF intensity around the first-coordination shell (<3.3 Å). In the second-coordination shell, corresponding to the peak centered at ∼4.0 Å in $g_{tot}(r)$, gGTI shows a less intense Ge-Ge second peak with respect to gGT4. These results are the first evidence of the disrupting role of iodine in the glass network, causing a decrease of the number of Ge-Te connections and Ge-Ge homopolar bonds. The shapes of the pair correlations functions become similar for intermediate range order distances ($r > 6$ Å).

For gGTI, the first peak of $g_{GeI}(r)$ contributes to the first main peak of the total $g_{tot}(r)$ (at ∼2.55 Å), along with additional contributions from $g_{GeTe}(r)$ and $g_{GeGe}(r)$. Instead, the first peak of the $g_{TeTe}(r)$ is the major contribution to the shoulder of the first main peak of $g_{tot}(r)$ (at ∼2.83 Å). This feature can be ascribed partially to Te-I distances, with a small bump at 2.86 Å in $g_{TeI}(r)$. However, Te-I distances contribute mainly to the second peak of the total $g_{tot}(r)$ (at ∼4.0 Å). In terms of nearest neighbor distances, Ge-Te and Ge-Ge are in good agreement with the experimental values (Table I). Although the original work of Jóvári *et al.* [7] on gGTI does not report any measurable value of the Ge-Ge bonding, the Ge-Ge bond distance in $Ge_{23.6}Te_{76.4}$ is fully compatible with the one we found in gGTI and gGT4. Indeed, the content of Ge-Ge homopolar bonds found by FPMD in both gGTI and gGT4 is on the verge of the accuracy of experimental probes (see Sec. II C for details).

C. Coordination number and local network environment

The coordination numbers $\bar{n}_{\alpha\beta}$ for Ge, Te, and I calculated for gGTI are listed in Table I. For comparison, the case of gGT4 is included. The partial coordination numbers are given in Table II. The coordination numbers $\bar{n}_{\alpha\beta}$ are defined as the average number of nearest neighbors of type β around an atom of type α within the range corresponding to the first minimum of the corresponding pair correlation function. Specifically, $\bar{n}$ reads $\bar{n} = c_{Ge}n_{Ge} + c_{Te}n_{Te} + c_{I}n_{I}$, where n_{Ge}, n_{Te}, and n_{I}, and c_{Ge}, c_{Te}, and c_{I} are the coordination numbers and the concentration of each species, respectively. The coordination numbers n_{Ge}, n_{Te}, and n_{I} are given by $n_{GeGe} + n_{GeTe} + n_{GeI}$, $n_{TeTe} + n_{TeGe} + n_{TeI}$, and $n_{II} + n_{IGe} + n_{ITe}$, for Ge, Te, and I atoms, respectively. For consistency, we use the same cutoff corresponding to the first minimum of the pair correlation function for both gGTI and gGT4. Looking at the coordination number n_{GeGe}, our gGTI model shows a value close to the one found in gGT4 (0.33 and 0.37). These values are slightly lower than the one found in $Ge_{23.6}Te_{76.4}$ by Jóvári *et al.* [16] (0.44) since gGTI has a slightly lower content of Ge. The

TABLE II. Distribution of the individual $\bar{n}_\alpha(l)$ structural units where an atom of species α (Ge, Te, or I) is l-fold coordinated to other atoms computed for the $Ge_{20}Te_{73}I_7$ and $Ge_{20}Te_{80}$ glasses. In bold are reported the total percentages determined for each l-fold coordination. These quantities have been calculated including neighbors separated by a cutoff corresponding to the first minimum in the $g_{\alpha\beta}(r)$. For the present work, the cutoffs used are 3.0, 3.15, 3.23, 3.1, and 3.4 Å for, respectively, the Ge-Ge, Ge-Te, Te-Te, Ge-I, and Te-I bonds. Only environments in a fraction >1% are reported.

		Proportions $\bar{n}_\alpha(l)$ (%)	
		$Ge_{20}Te_{80}$[a] FPMD	$Ge_{20}Te_{73}I_7$[b] FPMD
Ge atoms			
$l=3$		**7.46**	**18.50**
	Te_3	7.21	8.50
	Te_2I		7.94
	$GeTe_2$	0.25	1.54
$l=4$		**89.31**	**79.44**
	Te_4	61.23	41.71
	$GeTe_3$	21.10	14.93
	Te_3I		12.48
	Ge_2Te_2	6.98	5.71
	$GeTe_2I$		3.14
$l=5$		**3.11**	**1.19**
	$GeTe_4$	2.00	
	Te_5	1.11	
Te atoms			
$l=1$		**1.68**	**1.04**
$l=2$		**68.91**	**68.83**
	GeTe	27.18	31.24
	Te_2	26.40	24.61
	Ge_2	15.33	12.54
$l=3$		**26.60**	**26.93**
	$GeTe_2$	11.96	10.73
	Te_3	7.02	6.35
	Ge_2Te	6.50	5.69
	Ge_3	1.12	1.57
	Te_2I		1.37
	GeTeI		1.07
$l=4$		**2.38**	**2.72**
	$GeTe_3$	1.20	
I atoms			
$l=0$			**1.44**
$l=1$			**74.39**
	Ge		59.13
	Te		15.27
$l=2$			**23.33**
	GeTe		13.03
	Te_2		7.73
	Ge_2		2.57

[a]From Ref. [24].
[b]This work.

fact that in Ref. [16] both gGTI and glassy $Ge_{18.7}Te_{81.3}$ are not assigned any n_{GeGe} value can be ascribed to the lower limit of the characterization measurement employed (set in Ref. [16] at ∼0.3). The value of n_{GeTe} in the gGTI is lower than the one found in gGT4 (3.21 and 3.64), and this goes along with a concomitant formation of terminal Ge-I bonds ($n_{GeI} = 0.28$, in good agreement with the experimental value of 0.29). This behavior is indicative of a lower connectivity of the Ge-Te covalent network due to the inclusion of I. As a result the average coordination number of gGTI is found to be lower with respect to gGT4 ($\bar{n}_{gGT4}$: 2.65; $\bar{n}_{gGTI}$: 2.54). Conversely, the value of n_{TeTe} of gGTI is similar to the one of gGT4 (∼1.40).

As a further element of comparison between the two glasses, we note that gGTI exhibits an amount of fourfold Ge sites (∼79%) somewhat lower than the content found in gGT4 (∼89%). Among these fourfold atoms, 15.6% belong to mixed-anion units carrying one I atom, at variance with gGT4 ($Ge\text{-}Te_3I$ and $Ge\text{-}GeTe_2I$). The content of undercoordinated Ge increases in gGTI, for which threefold Ge sites have a similar content of $Ge\text{-}Te_3$ and $Ge\text{-}Te_2I$ units (∼8%). Also, the amount of twofold Te in the gGTI is very similar to the one found in gGT4 (68.8% and 68.9%). In most of the cases, I is coordinated to one neighboring atom (∼74.4%), preferentially forming a terminal Ge-I bond (∼59.1%). Although a non-negligible faction (23.3%) of twofold coordinated I is found in Ge-I-Te connections (∼13.0%), some minor Te-I-Te and Ge-I-Ge connections have been observed.

As shown in Table I, the percentage of Te atoms involved in homopolar bonds features similar values in gGTI and gGT4, in a way consistent with a coordination number $n_{TeTe} \sim 1.4$. It appears that the replacement of Te with I induces the formation of mixed-anion fourfold Ge units and an increase of mixed-anion threefold Ge units. This effect promotes a larger fraction of the Te-Te-Ge connections and a related decrease in the relative amount of the Te-Te-Te and Ge-Te-Ge connections. Therefore, in glasses with a significant excess of Te, I atoms preferentially break Ge-Te bonds in Te-Te-Ge and Ge-Te-Ge chains and terminate them mainly with Ge-I bonds, plus a minor contribution of Te-I connections. Hence, available Te atoms left undercoordinated can form Te-Te-Te linkages. Figure 3(a) shows a representative subset of the major structural units around Ge and Te atoms found in gGTI.

D. Bond angle distributions and order parameter

The bond angle distributions of triads centered around the Te atoms (shown in Fig. 4, Ge-Te-Ge being the most representative of a tetrahedral order) reflect the connectivity among the structural units (with presence or absence of departures from the Ge-Te-Ge linkages) and the presence of Te chains. Table I shows that corner-sharing (CS) connections are more numerous than edge-sharing (ES) connections. In Ge-S and Ge-Se chalcogenides, these two kinds of connections correspond to angles close to ∼103°/∼100° (CS) and ∼83°/∼90° (ES), respectively. In the present case, we observe a main peak around ∼93°, as the result of a ES small peak centered at ∼103° and a major peak centered at ∼94.5°. These results point out a major structural difference between Te-based and S-based and Se-based chalcogenides having Ge as the tetrahedral predominant atom. Focusing on the Te-Te-Te and Te-Te-I bond angle distribution functions, we observe the presence of a double peak profile (at 90° and 170°). In these cases, one has to account for the presence of Te chains or Te-Te-I units. The higher intensity at 170° for the Te-Te-I case reflects the presence at the tails of the chains of most of the I atoms bonded to

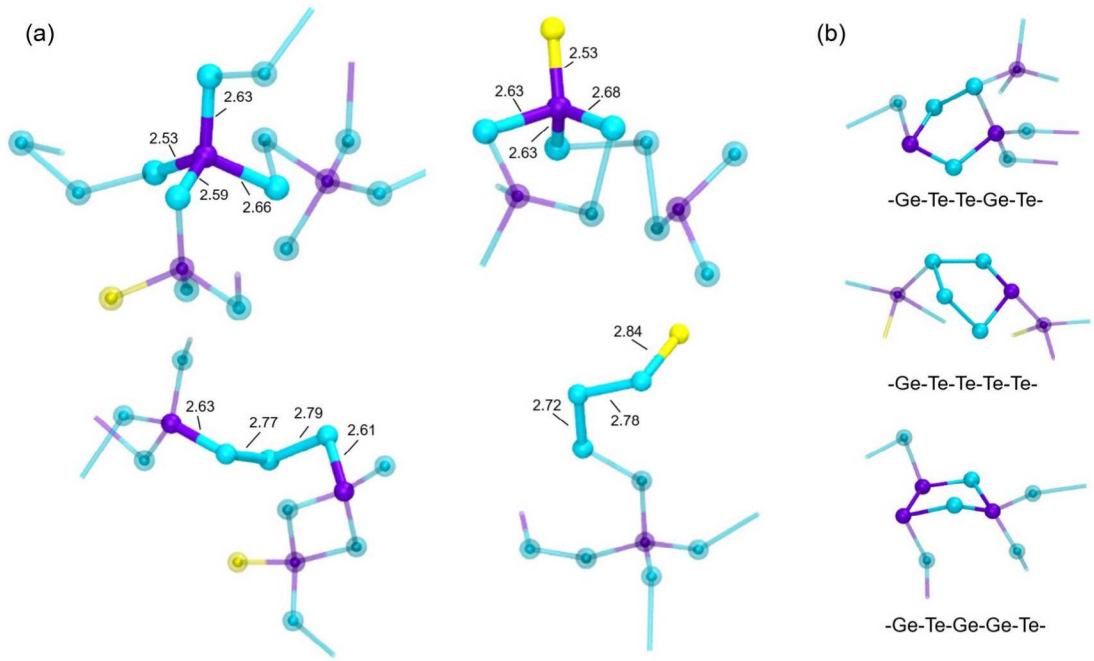

FIG. 3. (a) A representative subset of the structural units around Ge and Te atoms found in gGTI, where Ge atoms are purple, Te atoms are cyan, and I atoms are yellow. The following units are shown: $GeTe_4$ tetrahedra, $GeTe_3I$ mixed-anion tetrahedra, Te-Te-Te chain connecting two Ge-Te_4 units, and a terminal Te-Te-Te-I connection. The neighboring atoms are faded in light colors for clarity and the relevant bond distances are reported on the figure (Å). (b) The three most frequent types of five-member rings in gGTI.

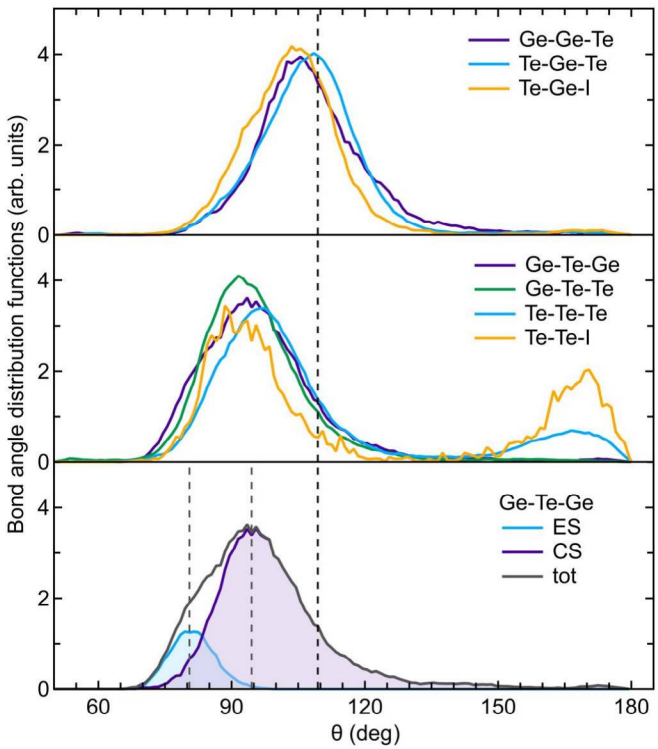

FIG. 4. Bond angle distributions functions (BAD) centered on Ge (top) and Te (middle) atoms. We also show the Ge-Te-Ge BAD which is decomposed in edge-sharing (ES) and corner-sharing (CS) contributions (bottom). The vertical black dashed line corresponds to 109.4° and the vertical gray dashed lines to the maximum of the ES (80.5°) and CS (94.5°) contributions.

Te atoms. The Te-Ge-Te bond angle distribution (and those in which Ge and I enters in defective connections, Ge-Ge-Te and Te-Ge-I) has its main peak centered at ∼109°. This is a well-known fingerprint of a tetrahedral network topology, observed when the majority of Ge atoms is connected in a tetrahedral fashion. The absence of any peak at 180° is indicative of the absence of defective octahedral Ge sites.

Further information on the atomic structure can be deduced from the order parameter $q = 1 - \frac{3}{8}\sum_{i>k}(\frac{1}{3} + \cos\theta_{ijk})^2$. This quantity is able to quantify the different weight of distinct coordination, the sum running over the bonded atom pairs where j is the central atom forming a bonding angle θ_{ijk} with its neighbors. For a perfect tetrahedron, the order parameter is $q = 1$, while $q = 0$ refers to an octahedral environment. A defective octahedron corresponds to $q = 5/8$ for fourfold coordination and $q = 7/8$ for threefold pyramidal ones. The peak at $\sim 0.95z$ in Fig. S4 (see SM) indicates that the majority of fourfold Ge sites has a tetrahedral configuration, while the small broadening up to $q = 0.65$ is due to defective fourfold Ge. The broad distribution in the range $q = 0.75$–0.95 for the threefold Ge is a signature of trigonal pyramidal coordination for these defective Ge sites.

E. Chains and rings statistics

On the basis of the results presented in the previous sections, gGTI and gGT4 result from a co of Ge-centered tetrahedra and Ge-Ge, Te-Te homopolar bonds. For each system, a deeper insight into the network organization can be obtained by resorting to the statistics of chains and rings. The role of chains is particularly relevant for amorphous Te

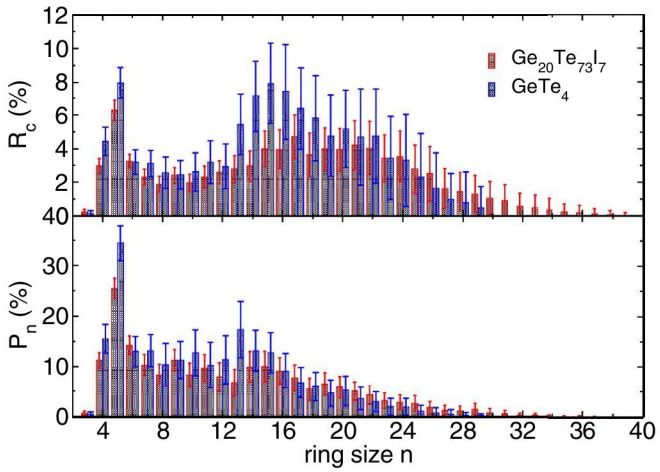

FIG. 5. Connectivity profiles, including standard deviations, for gGTI and gGT4 glasses calculated using the RINGS method. Top: $R_c(n)$, number of rings of size n normalized to the total number of atoms in the model. Bottom: $P_n(n)$, number of atoms at the origin of at least one ring of size n normalized to the total number of atoms in the model.

and Te-rich glasses as they are known to display a strong tendency for crystallization upon supercooling. This behavior results from the promotion of non-negligible secondary bonding interactions between adjacent $[Te]_n$ chains [48,49]. In the present work, the chains statistics is analyzed in terms of distribution of the individual $\bar{n}_\alpha(l)$ structural units reported in Table II. The existence of a sizable content of both linear and cross-linked chains is exemplified by the relative large amount of twofold coordinated -Te-**Te**-Te- chains (26.4% and 24.6% for gGT4 and gGTI, respectively) and threefold coordinated -Te-**Te**-$(Te)_2$ chains [7.0% (gGT4) and 6.4% (gGTI)]. The fact that gGT4 and gGTI glasses show a similar total content of linear and cross-linked chains means that the higher stability (weakened crystallization tendency) of gGTI glass with respect to gGT4 may be due to a different distribution of chains in terms of lengths, with gGTI having a greater content of shorter $[Te]_n$ chains.

To implement the rings analysis, the connectivity profiles were obtained via the rigorous investigation of networks generated using simulation (RINGS) code (Fig. 5) [50,51]. For comparison, we also report the rings analysis obtained for gGT4. Cutoff distances used to determine the nearest neighbors are those reported in Table II. The analysis is performed by making a shortest path search as implemented via the King [52]-Franzblau [53] method. This allows identifying rings containing a maximum of 40 and 30 atoms for gGTI and gGT4, respectively. In our procedure, we considered all atoms as initial points to begin the search for a given ring. Homopolar bonds are also taken into account. We define $R_c(n)$ as the number of rings containing n atoms (Ge, Te, or I) and $P_n(n)$ as the number of atoms that can be used as the origin of the search for at least one ring containing n atoms. Both quantities are normalized to the total number of atoms in our model. The first information provided by Fig. 5 is the existence of odd-membered rings in all sizes between 3 and 40 atoms. This result is due to the presence of Ge-Ge and Te-Te homopolar bonds. $R_c(n)$ is characterized by two distinct patterns. For relatively low values of n, one main peak arises, corresponding to small rings containing five atoms. This peak is due to rings with at least one Ge-Ge or Te-Te homopolar bond. Figure 3(b) shows the most recurrent types of five atoms rings of gGTI: Ge-Te-Ge-Te-Te (∼53%), Ge-Te-Te-Te-Te (∼26%), and Ge-Te-Ge-Ge-Te (∼13%). For n ranging between 10 and 40, a rather broad distribution becomes visible, with a maximum around 20 atoms per ring. The case of gGT4 shows a similar trend with the only noticeable difference in the maximum of the broad distribution centered at 15 atoms per rings. However, we remind that error bars affect the results for gGT4 at large ring sizes because of the relatively small size of the simulated model (215 atoms) [24]. Focusing on the network picture provided by $P_n(n)$, we remark that rings containing five atoms are the shortest paths for almost a third and fourth of all atoms in gGT4 and gGTI, respectively. Hence, we can infer that these rings are the basic building blocks of the topological network for medium range distances in gGTI, although some larger ring sizes (as $n = 14$) do involve more than 10% of the atoms.

IV. CONCLUSIONS

Previous atomic-scale modeling works (based on reverse Monte Carlo scheme) on disordered Ge-Te-X based systems have been shown to strongly depend on structural pre-assumptions or experimental information. While those results remain a useful reference to compare with, with the present work on glassy $Ge_{20}Te_{73}I_7$, and in line with our previous works on $Ge_{20}Te_{80}$ [24] and $Ga_{10}Ge_{15}Te_{75}$ [25], we further demonstrated that first-principles molecular dynamics is intrinsically capable of describing realistically and quantitatively disordered chalcogenide and chalcohalide ternary systems without the need of any structural pre-assumptions or input from experimental results.

FPMD simulations of glassy $Ge_{20}Te_{73}I_7$, enriched by a comparative analysis carried out with glassy $Ge_{20}Te_{80}$, has shown that both networks are characterized by tetrahedral connections coexisting with by Te-Te or Ge-Ge homopolar bonds. Iodine plays a disruptive role within the network, lowering its connectivity via the replacement of Te atoms, thereby cleaving Ge-Te bonds. These cleaved bonds, in turn, become terminal Ge-I groups. A minor, yet not negligible and disregarded in previous works, fraction of iodine is also found to be part of Te-I bonds. The breaking of Ge-Te connections and the formation of terminal Ge(Te)-I bonds results in a lowering of the average coordination number of the glass, accompanied by an increase of undercoordinated Ge at the expense of fourfold coordinated Ge atoms. This structural effect occurs along with an increase of threefold coordinated Te atoms. Iodine is mostly present in the mixed-anion $GeTe_{4-x}I_x$ tetrahedron and in the $GeTe_{3-x}I_x$ trigonal pyramidal unit. The analysis of chains and rings statistics provide evidence for the presence of linear and cross-linked chains made of Te and five-members rings containing at least one homopolar bonding (Te-Te or Ge-Ge).

Our results offer a deeper and more detailed insight on the structural properties for the chalcohalide $Ge_{20}Te_{73}I_7$ glass

with respect to previous works. Taking advantage of the predictive performance of the proposed FPMD scheme in quantitatively assessing the structural properties of a glassy chalcohalide system, this study raises the interest to complement the obtained findings with a further study on its bonding and electronic properties. Indeed, the interplay between the strong (iono)covalent and secondary bonding interactions (such as weak chalcogen and halogen bonding [24,54–56]) still have to be assessed for this class of systems. Plus, this work opens the way to the investigation of other complex chalcohalide ternary glasses that allow us to insert a greater content of halogen with respect to $Ge_{20}Te_{73}I_7$ and that show great potential in optoelectronic, space optics, and gas sensing applications.

ACKNOWLEDGMENTS

We acknowledge financial support from the Agence National de la Recherche (ANR) within the framework of the project IRTeGlass No. ANR-14-CE07-0013-02. G.O. acknowledges the Seed Money program of Eucor-The European Campus (project MEDIA) for financial support. Calculations were performed by using resources from GENCI (Grand Equipement National de Calcul Intensif, Grants No. A0080906092 and No. A0080807670), the Pole HPC Équipe@Meso of the Université de Strasbourg and from the computing facility MCIA (Mesocentre de Calcul Intensif Aquitain) of the Université de Bordeaux and of the Université de Pau des Pays l'Aldour.

[1] J. S. Sanghera and I. D. Aggarwal, Active and passive chalcogenide glass optical fibers for IR applications: A review, J. Non-Cryst. Solids **256**, 6 (1999).

[2] A. Zakery and S. Elliott, Optical properties and applications of chalcogenide glasses: A review, J. Non-Cryst. Solids **330**, 1 (2003).

[3] B. Bureau, S. Maurugeon, F. Charpentier, J.-L. Adam, C. Boussard-Pledel, and X.-H. Zhang, Chalcogenide glass fibers for infrared sensing and space optics, Fiber Integr. Opt. **330**, 28 (2009).

[4] V. S. Shiryaev and M. F. Churbanov, Recent advances in preparation of high-purity chalcogenide glasses for mid-IR photonics, J. Non-Cryst. Solids **475**, 1 (2017).

[5] S. Dai, Y. Wang, X. Peng, P. Zhang, X. Wang, and Y. Xu, A review of mid-infrared supercontinuum generation in chalcogenide glass fibers, Appl. Sci. **8**, 707 (2018).

[6] A. A. Wilhelm, C. Boussard-Plédel, Q. Coulombier, J. Lucas, B. Bureau, and P. Lucas, Development of far-infrared-transmitting Te based glasses suitable for carbon dioxide detection and space optics, Adv. Funct. Mater. **19**, 3796 (2007).

[7] P. Jóvári, I. Kaban, B. Bureau, A. Wilhelm, P. Lucas, B. Beuneu, and D. Zajac, Structure of Te-rich Te-Ge-X (X= I, Se, Ga) glasses, J. Phys.: Condens. Matter **22**, 404207 (2010).

[8] X.-H. Zhang, J.-L. Adam, and B. Bureau, *Chalcogenide Glasses*, Springer Handbook of Glass (Springer, Cham, 2019), pp. 525–552.

[9] S. Danto, P. Houizot, C. Boussard-Pledel, X.-H. Zhang, F. Smektala, and J. Lucas, A family of far-infrared-transmitting glasses in the Ga-Ge-Te system for space applications, Adv. Funct. Mater. **16**, 1847 (2006).

[10] P. Lucas, Z. Yang, M. Fah, T. Luo, S. Jiang, C. Boussard-Pledel, M.-L. Anne, and B. Bureau, Telluride glasses for far infrared photonic applications, Opt. Mater. Express **3**, 1847 (2013).

[11] J. Sun, Q. Nie, X. Wang, S. Dai, X. Zhang, B. Bureau, C. Boussard, C. Conseil, and H. Ma, Structural investigation of Te-based chalcogenide glasses using Raman spectroscopy, Infrared Phys. Techn. **55**, 316 (2012).

[12] X. Wang, Q. Nie, G. Wang, J. Sun, B. Song, S. Dai, X. Zhang, B. Bureau, C. Boussard, C. Conseil, and H. Ma, Investigations of Ge-Te-AgI chalcogenide glass for far-infrared application, Spectrochim. Acta A **86**, 586 (2012).

[13] Z. Zhao, B. Wu, X. Wang, Z. Pan, Z. Liu, P. Zhang, X. Shen, Q. Nie, S. Dai, and R. Wang, Mid-infrared supercontinuum covering 2.0–16 μm in a low-loss telluride single-mode fiber, Laser Photonics Rev. **11**, 170000513.3 (2017).

[14] W. Zhu, B. Aitken, and S. Sen, Structural mechanism of iodine incorporation in As-Se-I glasses and its effects on physical properties, J. Non-Cryst. Solids **478**, 79 (2017).

[15] W. Zhu, M. Lockhart, B. Aitken, and S. Sen, Dynamical rigidity transition in the viscoelastic properties of chalcogenide glass-forming liquids, J. Non-Cryst. Solids **502**, 244 (2018).

[16] P. Jóvári, A. Piarristeguy, A. Pradel, I. Pethes, I. Kaban, S. Michalik, J. Darpentigny, and R. Chernikov, Local order in binary Ge-Te glasses-An experimental study, J. Alloys. Compd. **771**, 268 (2019).

[17] I. Pethes, A. Piarristeguy, A. Pradel, S. Michalik, R. Nemausat, J. Darpentigny, and P. Jóvári, Short range order and topology of $Ge_xGa_xTe_{100-2x}$ glasses, J. Alloys. Compd. **834**, 155097 (2020).

[18] G. Ori, C. Massobrio, A. Bouzid, M. Boero, and B. Coasne, First-principles molecular dynamics study of glassy GeS_2: Atomic structure and bonding properties, Phys. Rev. B **90**, 045423 (2014).

[19] Z. Chaker, G. Ori, C. Tugene, S. L. Roux, M. Boero, C. Massobrio, E. Martin, and A. Bouzid, The role of dispersion forces on the atomic structure of glassy chalcogenides: The case of $GeSe_4$ and GeS_4, J. Non-Cryst. Solids **499**, 167 (2018).

[20] E. Lampin, A. Bouzid, G. Ori, M. Boero, and C. Massobrio, Impact of dispersion forces on the atomic structure of a prototypical network-forming disordered system: The case of liquid $GeSe_2$, J. Chem. Phys. **147**, 044504 (2017).

[21] A. Bouzid, G. Ori, M. Boero, E. Lampin, and C. Massobrio, Atomic-scale structure of the glassy $Ge_2Sb_2Te_5$ phase change material: A quantitative assessment via first-principles molecular dynamics, Phys. Rev. B **96**, 224204 (2017).

[22] A. Bouzid, H. Zaoui, P. L. Palla, G. Ori, M. Boero, C. Massobrio, F. Cleri, and E. Lampin, Thermal conductivity of glassy $GeTe_4$ by first-principles molecular dynamics, Phys. Chem. Chem. Phys. **19**, 9729 (2017).

[23] E. Martin, P. Palla, F. Cleri, A. Bouzid, G. Ori, S. L. Roux, M. Boero, and C. Massobrio, On the occurrence of size effects in the calculation of thermal conductivity by first-principles molecular dynamics: The case of glassy $GeTe_4$, J. Non-Cryst. Solids **498**, 190 (2018).

[24] A. Bouzid, C. Massobrio, M. Boero, G. Ori, K. Sykina, and E. Furet, Role of the van der Waals interactions and impact of the exchange-correlation functional in determining the structure of glassy $GeTe_4$, Phys. Rev. B. **92**, 134208 (2015).

[25] Z. Chaker, G. Ori, M. Boero, C. Massobrio, E. Furet, and A. Bouzid, First-principles study of the atomic structure of glassy $Ga_{10}Ge_{15}Te_{75}$, J. Non-Cryst. Solids **498**, 338 (2018).

[26] R. Car and M. Parrinello, Unified Approach for Molecular Dynamics and Density-Functional Theory, Phys. Rev. Lett. **55**, 2471 (1985).

[27] See http://www.cpmd.org/, copyright IBM Corp. 1990–2013, copyright MPI für Festkörperforschung Stuttgart 1997–2001.

[28] A. D. Becke, Density-functional exchange-energy approximation with correct asymptotic behavior, Phys. Rev. A **38**, 3098 (1988).

[29] C. Lee, W. Yang, and R. G. Parr, Development of the Colle-Salvetti correlation-energy formula into a functional of the electron density, Phys. Rev. B **37**, 785 (1988).

[30] N. Troullier and J. L. Martins, Efficient pseudopotentials for plane-wave calculations, Phys. Rev. B **43**, 1993 (1991).

[31] S. Nosé, A molecular dynamics method for simulations in the canonical ensemble, Mol. Phys. **52**, 255 (1984).

[32] S. Nosé, A unified formulation of the constant temperature molecular dynamics methods, J. Chem. Phys. **81**, 511 (1984).

[33] W. G. Hoover, Canonical dynamics: Equilibrium phase-space distributions, Phys. Rev. A **31**, 1695 (1985).

[34] G. J. Martyna, M. L. Klein, and M. Tuckerman, Nosé-hoover chains: The canonical ensemble via continuous dynamics, J. Chem. Phys. **97**, 2635 (1992).

[35] P. E. Blochl and M. Parrinello, Adiabaticity in first-principles molecular dynamics, Phys. Rev. B **45**, 9413 (1992).

[36] S. Grimme, Semiempirical GGA-type density functional constructed with a long-range dispersion correction, J. Comput. Chem. **27**, 1787 (2006).

[37] A. A. Wilhelm, C. Boussard-Pledel, P. Lucas, M. R. Riley, B. Bureau, and J. Lucas, New tellurium based glasses for use in bio-sensing applications, Proc. SPIE **6433**, 64330U (2007).

[38] Data deposited and available at the European Center of Excellence Novel Materials Discovery repository (nomad-repository.eu), DOI:10.17172/NOMAD/2020.11.24-2.

[39] See Supplemental Material at http://link.aps.org/supplemental/10.1103/PhysRevB.xx.xxxxxx for additional information about the computed structural properties obtained for GTI.

[40] A. C. Wright, The comparison of molecular dynamics simulations with diffraction experiments, J. Non-Cryst. Solids **159**, 264 (1993).

[41] I. Kaban, T. Halm, W. Hoyer, P. Jóvári, and J. Neuefeind, Short-range order in amorphous germanium-tellurium alloys, J. Non-Cryst. Solids **326–327**, 120 (2003).

[42] M. Sakurai, F. Kakinuma, E. Matsubara, and K. Suzuki, Partial structure analysis of amorphous $Ge_{15}Te_{80}M_5$ (M= Cu, Ag and In), J. Non-Cryst. Solids **312–314**, 585 (2002).

[43] S. Sen, S. Joshi, B. Aitken, and S. Khalid, Atomic structure and chemical order in binary Ge-Te and As-Te glasses: A Te K-edge x-ray absorption fine structure spectroscopic study, J. Non-Cryst. Solids **354**, 4620 (2008).

[44] P. Jóvári, P. Lucas, Z. Yang, B. Bureau, I. Kaban, and B. Beuneu, Short-range order in Ge-As-Te glasses, J. Am. Ceram. Soc. **97**, 1625 (2014).

[45] P. Jóvári, A. Piarristeguy, R. Escalier, I. Kaban, J. Bednarcik, and A. Pradel, Short range order and stability of amorphous Ge_xTe_{100-x} alloys ($12 \leqslant x \leqslant 44.6$), J. Phys.: Condens. Matter **25**, 195401 (2013).

[46] I. Kaban, P. Jóvári, W. Hoyer, and E. Welter, Determination of partial pair distribution functions in amorphous $Ge_{15}Te_{85}$ by simultaneous rmc simulation of diffraction and exafs data, J. Non-Cryst. Solids **353**, 2474 (2007).

[47] P. Jóvári, S. Cui, V. Nazabal, I. Kaban, B. Beuneu, M. Dussauze, C. Boussard-Pledel, and B. Bureau, Network rearrangement in AgI-doped $GeTe_4$ glasses, J. Am. Ceram. Soc. **98**, 1034 (2015).

[48] T. Chivers and R. S. Laitinen, Tellurium: A maverick among the chalcogens, Chem. Soc. Rev. **44**, 1725 (2015).

[49] B. Yuan, B. Aitken, and S. Sen, Rheology of supercooled Se-Te chain liquids: Role of Te as an interchain cross-linker, J. Non-Cryst. Solids **529**, 119764 (2020).

[50] S. L. Roux and P. Jund, Ring statistics analysis of topological networks: New approach and application to amorphous GeS_2 and SiO_2 systems, Comput. Mater. Sci. **49**, 70 (2010).

[51] S. L. Roux and P. Jund, Erratum: Ring statistics analysis of topological networks: New approach and application to amorphous GeS_2 and SiO_2 systems, Comput. Mater. Sci. **50**, 1217 (2011).

[52] S. V. King, Ring configurations in a random network model of vitreous silica, Nature (London) **213**, 1112 (1967).

[53] D. S. Franzblau, Computation of ring statistics for network models of solids, Phys. Rev. B **44**, 4925 (1991).

[54] G. Cavallo, P. Metrangolo, R. Milani, T. Pilati, A. Priimagi, G. Resnati, and G. Terraneo, The halogen bond, Chem. Rev. **116**, 2478 (2016).

[55] L. Vogel, P. Wonner, and S. Huber, Chalcogen bonding: An overview, Angew. Chem. Int. Ed. **58**, 1433 (2019).

[56] P. Scilabra, G. Terraneo, and G. Resnati, The chalcogen bond in crystalline solids: A world parallel to halogen bond, Acc. Chem. Res. **52**, 1313 (2019).